The thermal effect in diode-end-pumped continuous-wave 914-nm Nd:YVO_4 laser*

Yan Ren-Peng(闫仁鹏)[a)b)†], Yu Xin(于 欣)[a)b)], Chen De-Ying(陈德应)[a)b)], Chen Fei(陈 飞)[a)b)], Li Xu-Dong(李旭东)[a)b)], Ma Yu-Fei(马欲飞)[a)b)], and Yu Jun-Hua(于俊华)[a)b)]

[a)] *National Key Laboratory of Tunable Laser Technology, Harbin Institute of Technology, Harbin* 150080, *China*
[b)] *Institude of Opto-electronics, Harbin Institute of Technology, Harbin* 150080, *China*

(Received 13 June 2011; revised manuscript received 17 August 2011)

The thermal effect and the heat generation in diode-end-pumped continuous-wave 914-nm Nd:YVO_4 lasers are investigated in detail. A theoretical model of a diode end-pumped solid-state laser is constructed to analyse the influence of fractional thermal loading on the thermal effect in the Nd:YVO_4 laser based on finite element analysis. The thermal focal lengths and the end-surface deformations of laser rods in Nd:YVO_4 quasi-three-level and four-level lasers are measured and compared with the results obtained by ordinary interferometry for the demonstration of higher thermal loading in 914-nm laser. Finally the fractional thermal loading in the Nd:YVO_4 quasi-three-level laser is calculated by matching the experimental and the simulated end deformations.

Keywords: fractional thermal loading, Nd:YVO_4, 914-nm Nd:YVO_4 laser

PACS: 42.55.Xi, 42.60.Pk **DOI:** 10.1088/1674-1056/21/2/024208

1. Introduction

Lasers around 900 nm play an important role in many applications especially in generating blue lasers by frequency-doubling, which could be widely used in the fields of underwater communication, optical data storage, full color display, high resolution print and so on. As the most promising candidates for generating lasers around 900 nm, diode-end-pumped Nd^{3+}-doped quasi-three-level lasers have attracted much attention since first introduction by Fan and Byer in 1987.[1−3] While lasers around 1.06 μm emitting from the four-level transition have achieved high power and efficient output, the performance of quasi-three-level Nd^{3+}-doped lasers is not perfect enough, restricted mainly by some natural defects. First of all, the simulated emission cross ($\sim 10^{-20}$ cm^2) is only about 1/10 of the main four-level transition. Secondly the thermal population existing in the lower level leads to strong re-absorption of the oscillating laser.[4] To overcome the disadvantage and realize high power output in Nd^{3+}-doped quasi-three-level lasers high pump power intensity is required, which induces some inevitable negative influences on the laser performance. Primarily non-radiative process would be enhanced such as ground state absorption, energy-transfer upconversion (ETU) and excited-state absorption (ESA), which would result in additional heat generation and reduction of inverse population density.[5,6] The extra heat makes the temperature higher and the thermal lensing effect more serious in the laser rod than those in the four-level lasers, which is consequently the leading factor restricting the characteristics of Nd^{3+}-doped quasi-three-level lasers.

Due to the significant influence on the laser performance, many methods have been used to reduce the thermal effect in Nd^{3+}-doped quasi-three-level lasers.[7,8] However there has only been experimental study or theoretical estimation carried out on the thermal effect in Nd^{3+}-doped quasi-three-level lasers as done in four-level Nd^{3+}-doped lasers.[9−11] The extra heat generation in Nd^{3+}-doped quasi-three-level lasers, brought by the ESA and ETU effects has not been analysed quantificationally either, despite of its importance, which makes neither the fractional thermal loading determined nor the thermal effect evaluated precisely in Nd^{3+}-doped quasi-three-level lasers. The fractional thermal loading represents the fraction of absorbed pump power deposited as heat in

*Project supported by the National Natural Science Foundation of China (Grant No. 60978016), the Technological Project of Heilongjiang Province, China (Grant No. GC06A116), and the Fundamental Research Funds for the Central Universities, China (Grant No. HIT. NSRIF. 201165).

†Corresponding author. E-mail: yanrenpeng@yahoo.cn

© 2012 Chinese Physical Society and IOP Publishing Ltd

the laser medium at laser operation, which is a crucial factor in analysing the thermal effect of the solid-state lasers.[12−14] However the magnitude of fractional thermal loading in Nd^{3+}-doped quasi-three-level lasers is still ambiguous.[15,16]

In this paper the thermal effect and the heat generation in diode-end-pumped continuous-wave (CW) 914-nm Nd:YVO_4 lasers are investigated comprehensively. According to the theoretical finite element analysis (FEA) model in diode end pumped solid-state lasers the influence of fractional thermal loading on the thermal effect in the Nd:YVO_4 laser rod is demonstrated. A simple interferometry is used to measure the thermal focal lengths and end-surface deformations of laser rods in Nd:YVO_4 quasi-three-level and four-level lasers for the illustration of the serious thermal effect in the 914-nm laser, induced by the higher fractional thermal loading. Finally the fractional thermal loading with considering other nonlinear effects in 914-nm Nd:YVO_4 laser is evaluated by matching the experimental and simulated end-surface deformations.

2. Theoretic analysis on thermal effect in Nd:YVO_4 laser

In a diode-end-pumped lasers the temperature distribution ($T(x, y, z)$) and the thermal effect of the laser rod depend mainly on the heat flux induced by the pump power. The heat flux Poisson equation describing the relation between temperature distribution and heat flux is shown as follows:[17,18]

$$k \cdot \nabla^2 T(x,y,z) + \dot{q}(x,y,z) = 0, \tag{1}$$

where k is the heat conductivity of the laser rod and $\dot{q}(x,y,z)$ is the distribution function of heat flux transformed from the pump power. Considering the accuracy and for the simplification of the analysis, the pumping beam profile of a fiber-coupled diode-laser output is assumed to be approximately in multimode Gaussian distribution. The heat flux in the laser diode end pumped system could be expressed as

$$\dot{q}(x,y,z) = P_{\text{in}}\xi p(x,y,z)\frac{\alpha}{1-\exp(-\alpha z)} \times \exp(-\alpha z), \tag{2}$$

where ξ is the fractional thermal loading, α is the effective absorption coefficient, P_{in} is the incident pump power, and $p(x, y, z)$ is given by

$$p(x,y,z) = \frac{2}{\pi \cdot w_{\text{p}}^2(z)} \exp\left[\frac{-2(x^2+y^2)}{w_{\text{p}}^2(z)}\right], \tag{3}$$

where $\omega_{\text{p}}(z)$ is the normalized distribution of pump light

$$w_{\text{p}}(z) = w_{\text{p0}}\left\{1+\left[\frac{\lambda_{\text{p}} M_{\text{p}}(z-z_0)}{\pi n w_{\text{p0}}^2}\right]^2\right\}^{1/2}, \tag{4}$$

with ω_{p0} being the beam waist radius, z_0 the beam waist location, λ_{p} the pump wavelength, M_{p}^2 the beam quality. Since the contact between crystal and heat sink is not ideal, the temperature (T_{s}) at the edge of the laser crystal could not be equal to the temperature (T_{c}) of heat sink.[19] The realistic condition follows a Newton-type law of cooling and the conduction relation could be described as

$$-k\frac{\partial T}{\partial n} = h(T_{\text{s}} - T_{\text{c}}). \tag{5}$$

In addition, the thermal stresses in the radial and axis directions in the laser rod would be induced by the inevitable temperature gradient. According to thermoelasticity the mechanical stress and mechanical strain distribution is discussed here. The equations of equilibrium of stresses in the Cartesian coordinates are given by

$$\begin{aligned}
&\frac{\partial \sigma_{xx}}{\partial x} + \frac{\partial \sigma_{xy}}{\partial y} + \frac{\partial \sigma_{zx}}{\partial z} = 0,\\
&\frac{\partial \sigma_{xy}}{\partial x} + \frac{\partial \sigma_{yy}}{\partial y} + \frac{\partial \sigma_{yz}}{\partial z} = 0,\\
&\frac{\partial \sigma_{zx}}{\partial x} + \frac{\partial \sigma_{yz}}{\partial y} + \frac{\partial \sigma_{zz}}{\partial z} = 0,
\end{aligned} \tag{6}$$

where the stress components σ_{ii} and σ_{ij} ($i \neq j$) represent the normal component and the shear component respectively, with the subscript i or j denoting x, y, and z. The strain-displacement relationships are expressed as follows:

$$\begin{aligned}
&\varepsilon_{xx} = \frac{\partial u_x}{\partial x}, \quad \varepsilon_{xy} = \frac{1}{2}\left(\frac{\partial u_x}{\partial y} + \frac{\partial u_y}{\partial x}\right),\\
&\varepsilon_{yy} = \frac{\partial u_y}{\partial y}, \quad \varepsilon_{xy} = \frac{1}{2}\left(\frac{\partial u_y}{\partial z} + \frac{\partial u_z}{\partial y}\right),\\
&\varepsilon_{zz} = \frac{\partial u_z}{\partial z}, \quad \varepsilon_{zx} = \frac{1}{2}\left(\frac{\partial u_z}{\partial x} + \frac{\partial u_x}{\partial z}\right),
\end{aligned} \tag{7}$$

where ε_{ii} are direct strains in the x, y, and z directions and ε_{ij} ($i \neq j$) are shear strains, u_i are the displacements in the x, y, and z directions. Based on Hooker's law the strain–stress relations in anisotropic crystal is expressed as

$$\begin{aligned}
&\sigma_{xx} = 2\gamma\varepsilon_{xx} + \delta_{xx}[\zeta e - (3\zeta + 2\gamma)\alpha_a T(x,y,z)],\\
&\sigma_{yy} = 2\gamma\varepsilon_{yy} + \delta_{yy}[\zeta e - (3\zeta + 2\gamma)\alpha_c T(x,y,z)],\\
&\sigma_{zz} = 2\gamma\varepsilon_{zz} + \delta_{zz}[\zeta e - (3\zeta + 2\gamma)\alpha_c T(x,y,z)],\\
&\sigma_{xy} = 2\gamma\varepsilon_{xy}, \quad \sigma_{yz} = 2\gamma\varepsilon_{yz},
\end{aligned}$$

$$\sigma_{xz} = 2\gamma\varepsilon_{xz}, \tag{8}$$

where δ_{ii} is the Kronecker delta function; $T(x, y, z)$ is the temperature distribution in the laser rod, solved based on Eq. (1); e is the sum of normal strains ($e = \sum \varepsilon_{ii}$); α is the thermal expansion coefficient; ζ and γ are the constants related to the mechanical properties of the laser crystal, which are expressed with Young's modulus E and Poisson ratio v as follows:

$$\zeta = \frac{\nu E}{(1+v)(1-2v)}, \tag{9}$$

$$\gamma = \frac{E}{2(1+v)}. \tag{10}$$

It is obvious that the Young's modulus E and Poisson ratio v play an important role in analysing the mechanical performance of the laser rod. In the following experiment the values of these parameters would also be evaluated with the interferometry to keep the consistence of our research. Based on Eqs. (1)–(10) a theoretical model can be constructed to analyse the thermal effect in the laser rod based on FEA. The significant factors related to the thermal effect such as temperature, stress density distribution and end-surface deformation in the laser rod can be simulated with the ANSYS software.

Figure 1 shows the simulated temperature distribution in the pumping end surface in the Nd:YVO_4 laser. In the simulation the fractional thermal loading is assumed to be $\xi = 30\%$ and other main parameters are shown in Table 1. The maximum temperature emerges in the centre of the pumping light, which reaches 61 °C much bigger than the side-surface temperature. It can be seen that the variations of temperature gradients in different directions are not obvious regardless of the different values of thermal condition. With the supposed Young's modulus and Poisson ratio ($E = 134$ Gpa and $v = 0.33$) the simulated mechanical and thermal stress density and deformation in the pumping end surface of the Nd:YVO_4 laser rod are shown in Fig. 2. Being different from the case of the isotropous temperature distribution there is remarkable difference of mechanical performance between horizontal and vertical directions, which is attributed to the distinct anisotropic mechanical property of Nd:YVO_4 crystal.

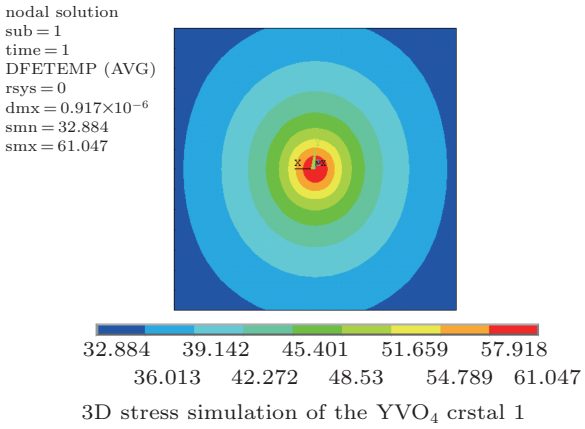


Fig. 1. (colour online) Simulated temperature distribution in the pumping end surface of the Nd:YVO_4 laser rod.

Table 1. Main parameters in the FEA simulation.

	Description	Value
Pump parameters	Pump wavelength λ_p/nm	808
	Incident pump power P_{in}/W	20
	Effective absorption coefficient α/m^{-1}	183.3
	Beam quality factor M_p^2	144
	Beam waist radius $\omega_{p0}/10^{-4}$ m	200
	Beam waist location $z_0/10^{-3}$ m	1
Crystal parameters	Dimension/10^{-9} m^3	6(L)×3(W)×3(H)
	Thermal conductivity k/(W/(m·K))	8.5 (a axis)[20] 11.2 (c axis)[20]
	Specific heat c_p/(J/(g·K))	0.429
	Refractive index n	1.972 (a axis) 2.165 (c axis)
	Thermal-expansion coefficient/ 10^{-6} K^{-1}	4.43 (a axis) 11.37 (c axis)
	Thermal-optical coefficient/10^{-6} K^{-1}	3.0 (a axis) 8.6 (c axis)
Boundary conditions	Side-surface temperature T_s/K	305
	Ambient temperature T_s/K	295
	Boundary heat transfer coefficient h/(W/(m^2·K))	15000

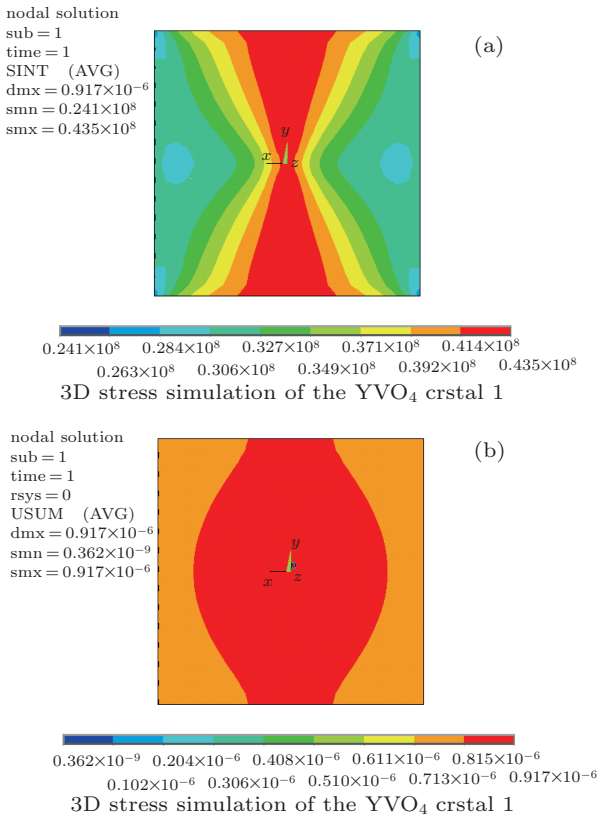


Fig. 2. (colour online) Mechanical and thermal stress densities (a) and surface deformation distribution (b) in the pumping end surface of the Nd:YVO_4 laser rod.

From the above analyses it is obvious that the thermal effect in the laser rod depends mainly on fractional thermal loading ξ in laser operation under the same pumping condition. On the basis of the FEA simulation the effects of fractional thermal loading on the maximum temperature and end-surface deformation in the Nd:YVO_4 crystal are given in Fig. 3. With the increase of fractional thermal loading the maximum temperature and the end-surface deformation in the pumping end of laser rod are enhanced greatly. Fractional thermal loading represents the inevitable and needless heat generation in laser operation and its value could be assumed to be equal to quantum deficiency as expressed below if the other nonradiative effect is neglected:

$$\xi = 1 - \lambda_{\rm p}/\lambda_l. \tag{11}$$

In the Nd:YVO_4 four-level laser pumped at 808 nm the quantum deficiency is supposed to be 24%.[21] However for the quasi-three-level operation the simulated emission cross is so small that the other effects (reabsorption, ETU, and ESA) inducing extra heat generation may not be ignored, which makes the value much bigger than the quantum deficiency of 11.6% in Nd:YVO_4 914-nm laser. In the following experiment the serious thermal effect in Nd:YVO_4 quasi-three-level laser is investigated comprehensively and the value of fractional thermal loading is determined.

3. Measurement of the thermal effect and determination of fractional thermal loading in Nd:YVO_4 quasi-three-level laser

3.1. Experimental setup and analysis

The setup schematic of diode-end-pumped CW Nd:YVO_4 laser and interferometer equipment for measuring the end-surface deformation and the thermal focal length is shown in Fig. 4. The pump source is a 50-W fiber-coupled laser diode emitting at 808 nm and the pump beam is focused into the laser medium with a beam waist radius of 200 μm. A 0.1at% Nd^{3+}-doped Nd:YVO_4 rod with a dimension of 3 mm×3 mm×6 mm serves as the laser medium. The laser rod is wrapped with indium foil and mounted in the copper heat sink to dissipate the extra heat from laser operation. The front facet of the laser rod was coated with high reflectivity (HR) at 914 nm ($T > 99.8\%$) and high transmissivity (HT) at 808 nm ($T > 99\%$), which can be employed as the rear mirror when the end-surface deformation in 914-nm laser is measured. Antireflection is coated at 1064 nm ($R < 5\%$) and 1342 nm ($R < 10\%$) on both faces to prevent parasitical oscillating. The plane mirror M1 and the concave mirror M2 are the rear mirror and the output mirror respectively. The length of the laser cavity is adjusted according to the variable measured. The same interferometer measurement system is adopted in the whole measuring process. The probe beam is produced from an He–Ne laser and the solid line and dashed line in the scheme show the beam paths for measuring the end-surface deformation and the thermal focal length in the laser rod. A glass is employed to split the probe beam into two paths, one is the object beam (beam 1) and the other is the reference beam (beam 2) when the pumping end deformation is measured. The rear surface of the laser rod serves as the beam splitter to measure the phase change caused by thermal lens effect. The two split beams are combined after a focusing lens and the typical interferogram is collected by a CCD camera, which is presented in the insert of Fig. 1. The fringes move with the variation of optical path difference (OPD) between the two split beams (2 and 3, or 2′ and 3′),

which carry the information about end-surface deformation and thermal focal length.

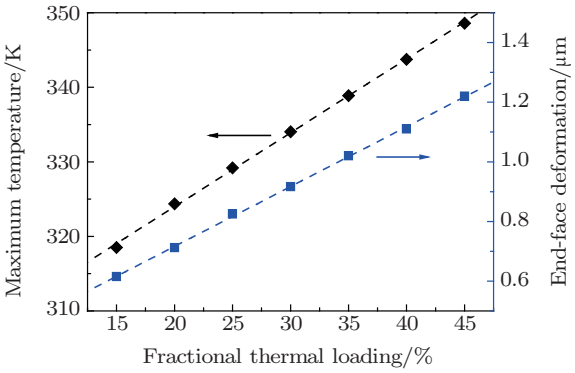


Fig. 3. (colour online) Maximum temperature and end-surface deformation in the pumping end of Nd:YVO_4 crystal versus fractional thermal loading.

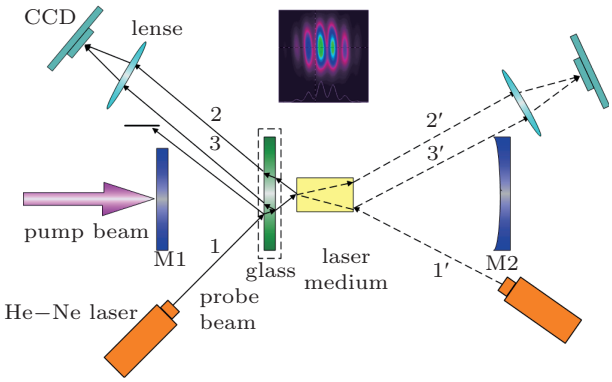


Fig. 4. (colour online) Schematic diagram of experimental setup.

With the shifted number of fringe, the phase variation of two beams could be obtained and also the focal thermal length and end-surface deformation acquired. The total OPD between beams ($2'$ and $3'$) induced by the thermal effect in the whole rod can be expressed by the change of the refractive index and end-surface deformation in the laser rod as

$$\mathrm{OPD} = L\Delta n + n\Delta L, \tag{12}$$

where Δn and ΔL represent the variations of refractive index and end-surface deformation respectively. Therefore the interferogram contains the comprehensive information about both index and end changes induced by the thermal effect. If the thermal lens in the laser rod is assumed to be an ideal thin lens to simplify the calculation, the focal length of this spherical thin lens could be given by[22]

$$f_{\mathrm{th}} = \frac{r^2}{2\cdot[\mathrm{OPD}(r) - \mathrm{OPD}_0]}, \tag{13}$$

where OPD_0 is the OPD on the optical axis, and r is the distance from optical axis. It should be mentioned that the f_{th} is an averaged thermal lens obtained in the parabolic profile. Then there exists a relationship between the magnitude of thermal lens and the change of interference fringes. Based on the theory of light transmission optics, the thermal focal length can be related to the phase variation as follows:

$$f_{\mathrm{th}} = \frac{R^2\cos\theta}{m\lambda}, \tag{14}$$

where R is the radius of pump region, θ is the incident angle of probe beam, λ is the wavelength of probe beam, and m is the number of interfere fringe variation.

Similarly, by the variation of OPD between light beams (2 and 3) the magnitude of end-surface deformation in the pumping surface is obtained by[23]

$$d = \frac{m\lambda}{2\cos(\theta)}. \tag{15}$$

3.2. Experimental results and discussion

In the experiment the thermal effect in Nd:YVO_4 four-level laser and that in quasi-three-level transition are measured, through which the serious thermal effect induced by higher thermal loading in 914-nm laser can be described clearly. On the basis of Eq. (13) the thermal focal lengths in 914-nm and 1064-nm laser operating conditions versus input pump power are obtained as shown in Fig. 5. It is obvious that with the increase of the input pump power the thermal focal length becomes shorter and the thermal focal length in 914-nm laser operation is several times smaller than that in 1064-nm laser under the same condition and power. The thermal focal length in 914-nm laser becomes even smaller than 50 mm when the pump power is higher than 20 W, by which the serious thermal effect in 914-nm Nd:YVO_4 laser operation is demonstrated. According to Eq. (2), the difference indicates that fractional thermal loading is much higher in quasi-three-level Nd:YVO_4 laser than in 1064-nm laser.

For further illustration the end-surface deformations of Nd:YVO_4 laser rod in different laser operating conditions are determined as shown in Fig. 6. The maximum end-surface deformations are 2.1 μm, 1.87 μm, and 1.49 μm at the input pump power of 28 W during non-laser, 914-nm laser and 1064-nm laser operations respectively. The end deformations in 1064-nm and 914-nm laser operations are 30% and 10% lower than that of non-laser operation, which

could be attributed to the reduction of heat generation by the energy extraction of laser operation. The phenomenon could also be explained that the variation scale of end deformation in 914-nm laser operation changes after threshold. The data also illustrates that heat generation in 914-nm laser is bigger than that in 1064-nm laser and the nonlinear progress as the heat source should also be considered in 914-nm Nd:YVO_4 laser except for quantum deficiency.

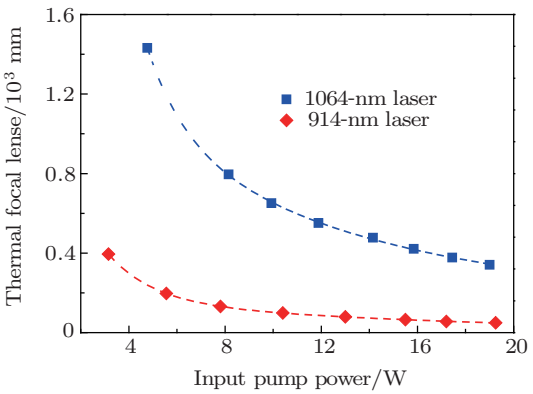


Fig. 5. (colour online) Thermal focal lengths in 914-nm and 1064-nm Nd:YVO_4 lasers versus input pump power.

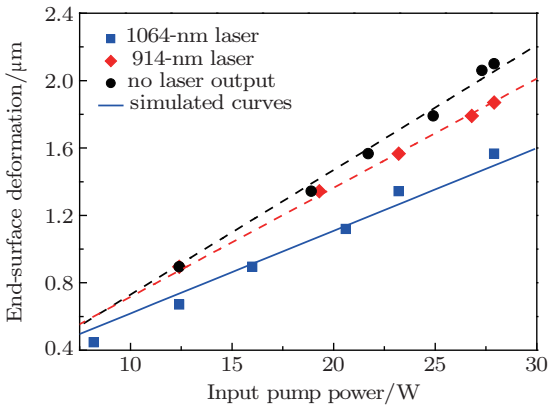


Fig. 6. (colour online) End-surface deformations of Nd:YVO_4 rod in different laser operations versus input pump power.

Through the comparison between experimental data and numerical simulation based on the FEA model, the values of Poisson ratio and Yong's modulus of Nd:YVO_4 crystal are also obtained. In the simulation the fractional thermal loading in 1064-nm laser operation is supposed to be 24% ($\xi_{1064\ \mathrm{nm}} = 24\%$). When the Poisson ratio and the Yong's modulus of Nd:YVO_4 crystal are assumed to be 0.33 GPa and 134 GPa respectively, the simulated end-surface deformation (solid line) in 1064-nm Nd:YVO_4 laser matches experimental result well as shown in Fig. 5. The magnitudes of Poisson ratio and Yong's modulus can be estimated to be 0.33 GPa and 134 GPa in Nd:YVO_4 crystal respectively.

With the estimated mechanical property of Nd:YVO_4 crystal the fractional thermal loading in 914-nm Nd:YVO_4 laser is evaluated by matching the FEA result of end-surface deformation with experimental data. The calculated fractional thermal loading in the laser rod as a function of input pump power is shown in Fig. 7. The ratio increases first with the pump power increasing and then maintains a constant of 32% when the threshold is reached. The initial increase could be ascribed to the difference between the wavelength of pumping light and the absorbed peak wavelength of laser medium at the lower pump region. Besides, the value of 32% is nearly three times higher than the quantum deficiency of 11.6% in the Nd:YVO_4, so another relaxation process accounts for a significant amount of extra thermal loading being generated. The thermal loading could be interpretative for the serious thermal effect qualitatively. The factors leading to the heat generation requires additional detailed analysis. It is important to mention that the evaluated fractional thermal loading in 914-nm Nd:YVO_4 laser is a relative magnitude according to supposed thermal loading of 24% in 1064-nm laser.

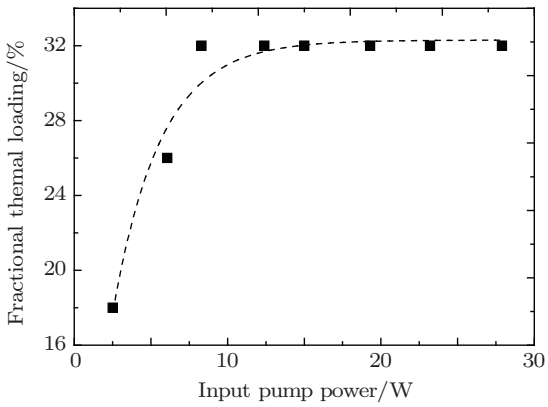


Fig. 7. Fractional thermal loading of Nd:YVO_4 quasi-three-level laser versus input pump power.

4. Conclusion

Comprehensive investigations on the thermal effect and heat generation in Nd:YVO_4 quasi-three-level laser are conducted. The thermal effect in Nd:YVO_4 laser medium and the influence of fractional thermal loading on thermal effect are simulated by theoretical FEA model. To further demonstrate serious thermal effects in 914-nm Nd:YVO_4 laser generated by higher thermal loading the thermal focal lengths and the end-surface deformations in different laser operations are

measured and compared with each other. Through matching the experimental and the simulated end-surface deformation the fractional thermal loading coefficient in 914-nm Nd:YVO_4 laser is evaluated to be approximately a constant of 32%, which is about 30% higher than that in 1064-nm laser. Detailed research is needed to determine the progress of the nonlinear effect generating heat.

References

[1] Fan T Y and Byer R L 1987 *IEEE J. Quantum Electron.* **23** 605

[2] Risk W and Lenth W 1988 *Opt. Lett.* **12** 993

[3] Zeller P and Peuser P 2000 *Opt. Lett.* **25** 34

[4] Chen F, Yu X, Li X D, Yan R P, Wang C, Luo M, Peng J B, Zhang Z H and Yu J H 2009 *Opt. Commun.* **283** 3755

[5] Bjurshagen S and Koch R 2004 *Appl. Opt.* **43** 4753

[6] Fornasiero L, Kück S, Jensen T, Huber G and Chai B 1998 *Appl. Phys.* B **67** 549

[7] Yu X, Yan R P, Luo M, Chen F, Li X D and Yu J H 2009 *Laser Phys.* **19** 1960

[8] Lü Y F, Zhang X H, Yin X D, Xia J, Zhang A F and Lin J Q 2010 *Appl. Phys.* B **99** 115

[9] Chang Y T, Huang Y P, Su K W and Chen Y F 2008 *Opt. Express* **16** 21155

[10] Song F, Zhang C, Ding X, Xu J and Zhang G 2002 *Appl. Phys. Lett.* **81** 2145

[11] Zhou C 2009 *Chin. Phys.* B **18** 1547

[12] Chen Y F 1999 *IEEE J. Quantum Electron.* **35** 234

[13] Zhang X L, Wang Y Z, Li L and Ju Y L 2007 *J. Phys.* D: *Appl. Phys.* **40** 6930

[14] Song F, Liu S, Wu Z, Cai H, Zhang X, Teng L and Tian J 2007 *J. Opt. Soc. Am.* B **24** 2327

[15] Krennrich D, Knappe R, Henrich B, Wallenstein R and L'Huillier J A 2008 *Appl. Phys.* B **92** 165

[16] Gao J, Yu X, Yan R P, Gu H D, Zheng C Q, Wu X D, Wei B, Chen F and Li X D 2009 *J. Russ. Laser. Res.* **30** 376

[17] Xiong Z, Li G, Moore N, Huang W L and Lim G C 2003 *IEEE J. Quantum Electron.* **39** 979

[18] Liu Q X and Zhang M 2010 *Acta Phys. Sin.* **59** 8535 (in Chinese)

[19] Song X L, Guo Z, Li B B, Wang S Y, Cai D F and Wen J G 2009 *Acta Phys. Sin.* **58** 1700 (in Chinese)

[20] Sato Y and Taira T 2006 *Opt. Express* **14** 10528

[21] Peng X, Asundi A, Chen Y and Xiong Z 2001 *Opt. Eng.* **40** 1100

[22] Weber R, Neuenschwander B, Mac Donald M, Roos M and Weber H 1998 *IEEE J. Quantum Electron.* **34** 1046

[23] Peng X, Asundi A, Chen Y and Xiong Z 2001 *Appl. Opt.* **40** 1396